Charged mode 97/99 analysis

S.Glazov

November 12, 2007

Contents

Chapter 1

Introduction

This document summarises results of the $K_L \to \pi^+\pi^-$ analysis performed on data collected in the years 1997 and 1999. An emphasis is made on the updates with respect to the previously published analysis [**?**]. These updates correspond to the charged mode reconstruction version **6.03**, also used for the measurement of the CKM parameter $|V_{us}|$ [**?**, **?**, **?**].

An outline of the document is as follows. The discussion starts with the description of the data analysis cuts and event yields. It is followed by an explicit list of the changes in the analysis with respect to the published result. An updated background subtraction procedure is explained next. The central value and statistical uncertainty for $Re(\epsilon'/\epsilon)$ is given in Chapter 3. The systematic uncertainties are discussed next. The determination of the neutral kaon system parameters and CPT invariance tests are reported in Chapter 4 Further details on the analysis are given in Appendices.

Chapter 2

Data Analysis

2.1 Data sample

Table 2.1

2.2 Changes vs Publication

2.2.1 Updates of the Kaon Propogation Simulation

Decays in the regenerator. Updated M_K value.

2.2.2 Updates of the Drift Chamber Spectrometer Simulation

Full tracing. Fringe field corrections. δ-ray simulation. Multiple scattering update.

2.2.3 Updates of the CsI Calorimeter Simulation

Update of the pion shower library - CIA veto.

Year	Vacuum Beam	Regenerator Beam
1997	10670688	18594207
1999	14447735	25115620
Total	25118423	43709827

Table 2.1: Number of events collected in 1997 and 1999 for Vacuum and Regenerator beam before background subtraction.

2.2.4 Updates in the Reconstruction

In drift cell dependent position resolution. DC geometry update.

2.2.5 Changes in Selection Cuts

X-separation at CsI. Tighter MA clearance cut. Track based geometrical validation of EWUD logic.

2.3 Background Subtraction

A new background subtraction procedure has been developed for this analysis. The main new features of this approach are:

- K_{e3} and $K_{\mu 3}$ components of the background are normalized separatelly using $M_{\pi\pi}$ and $p_\perp$ sidebands. The seperation is achieved on the basis of the calorimeter responce. "Double MIP sample", $E_\pi^{max} < 1??$ GeV is used for normalization of the $K_{\mu 3}$ background. Sample with both pion-candidates interacting hadronically, $E_\pi^{min} > 5??$ GeV is used for K_{e3} decays normalization.

- For $K_{\mu 3}$ background, the momentum dependent probability of the muon vetoing in the muon system is determined in data and explicitly taken into account. Previous analysis effectivelly corrected for this effect by E_K dependent background normalization.

- Additional background sources are considered in the regenerator beam. These are hadronic productions of K^* and Δ resonances via $K_L + N \to K_S^* + X$ and $n + N \to \Delta + X$. The incident neutron spectrum is considered to be the same as of the Λ baryon. For K_S^* decays, both $K^\pm\pi^\mp$ and $\pi^0 K_S, K_S \to \pi^+\pi^-$ modes are simulated. The $K_S^* \to \pi^0 K_S$ background is normalized using $P_\perp$ side band in regenerator beam. $K_S^* \to K^\pm\pi^m p$ and $\Delta \to p^\pm\pi^\mp$ decays are normalized using mass sidebands in the regenerator beam reconstructed with the vertex located at the regenerator edge. The two modes are seperated using momentum asymmetry distribution of the secondary particles.

Otherwise, the background subtraction follows the same algorithm as for the published result [**?**]. Namely:

Source	Background level, %					
	97 PRD		97		99	
	Vac	Reg	Vac	Reg	Vac	Reg
K_{e3}	0.036	0.001	0.032	0.001	0.032	0.001
$K_{\mu 3}$	0.054	0.002	0.034	0.001	0.030	0.001
Collimator scattering	0.010	0.010	0.009	0.009	0.008	0.008
Regenerator scattering	—	0.074	—	0.073	—	0.075
Total background	0.100	0.087	0.074	0.083	0.070	0.085

Table 2.2: Background fractions. Contributions of the other background sources is below 0.001%

- Collimator scattering component is normalized using tight $K \to \pi^+\pi^-$ selection for vacuum beam events, applying all but $p_\perp$ cuts. LARGE pt ? The reconstructed kaon is projected backwards along the kaon momentum direction to the location of the defining collimator, $Z = 88$ m. An accumulation of the events at the collimator edges is used then for normalization, see Fig B.2.

- Diffractive component of regenerator scattering is taken from BLA Inelastic component is normalized using $Z > X$.

- The normalization of the background components is determined in 10 GeV kaon momentum bins and than parameterized as a second order polynomial of E_K, see Fig. B.1 for the results.

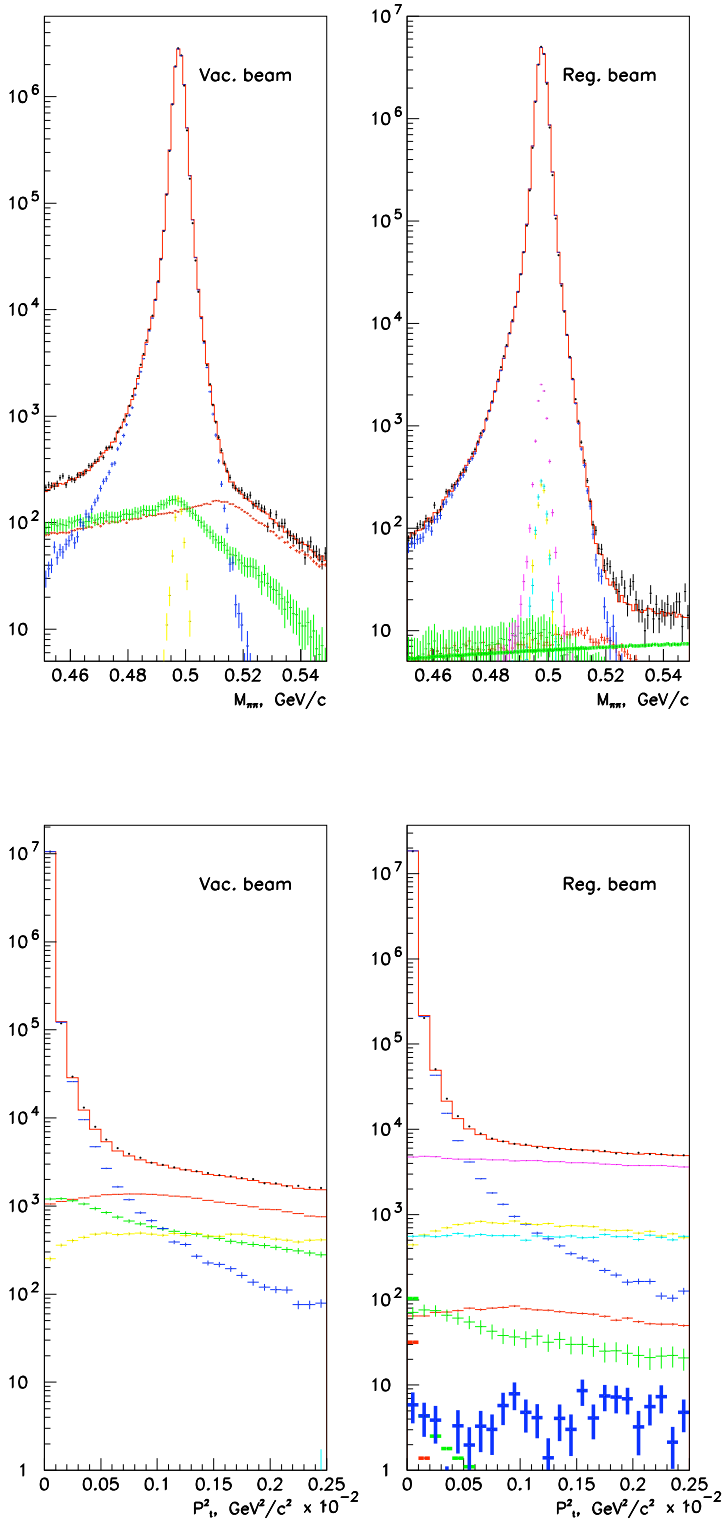

Figure 2.1: Mass and $P_\perp$ distributions for Vacuum and Regenerator beam for 1997 data

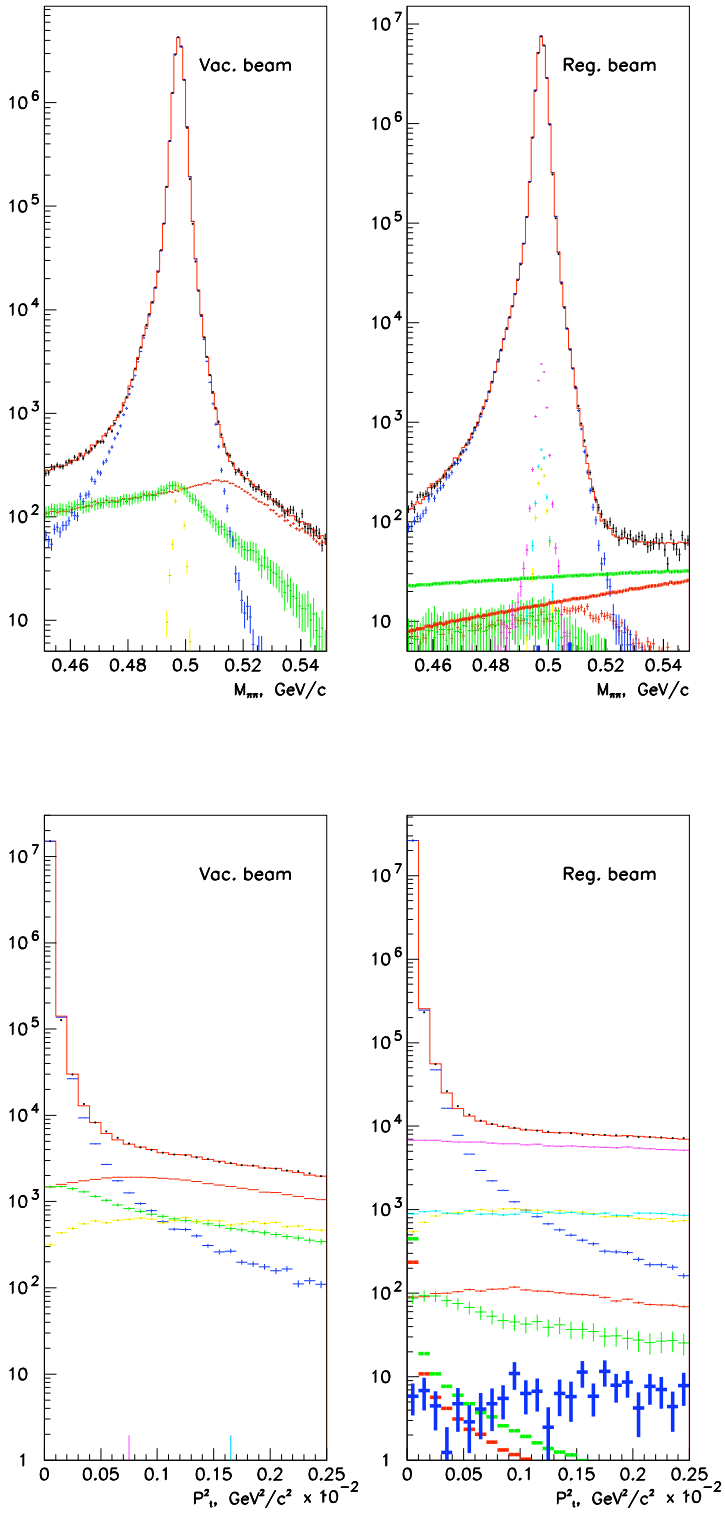

Figure 2.2: Mass and $P_\perp$ distributions for Vacuum and Regenerator beam for 1999 data

Chapter 3

$Re(\epsilon'/\epsilon)$ Results

3.1 Systematic Uncertainties

Systematic uncertainties in this analysis arrise from various sources which may influence differnetly data in the Vacuum compared to the Regenerator beam. These uncertainties are discussed in this section. Table 3.4 summarizes the systematic uncertainties.

3.1.1 Online Event Selection

L1, L2 bias have been studied elsewhere ??

To study L3 selection bias, events triggered by trigger B03 and random L3 accepts of trigger B01 are used. Table 3.1 summarizes the results of this study. The L3 bias found for 97 data (0.32 ± 0.20) has consistent uncertainty with the bias found for the published result (0.46 ± 0.20) but somewhat smaller central value. This discrepancy might be caused by the difference in the final selection criteria. Note that the total L3 uncertainty derrived from these two determinations of L3 loss, 0.42 versus 0.56, is not very different.

Figure 3.1 shows L3 induced loss for 99 data as a function of run number. The larger loss for runs < 13705 can be explained by different T3NML steering conditions. The five runs with large sporadic L3 loss are 14377,14383,14048,14505 and 14518. This loss is consistent for Vac and Reg beam data and also for B03 reference sample. If the five runs are exluded from the analysis, the L3 bias is reduced to 0.28 ± 0.14. We chose to exclude these runs for the final arrays. The combined 97-99 loss given in Table 3.1 is based on the sample with these runs excluded.

Reference Trigger	Bias in $Re(\epsilon'/\epsilon)$			
	97	99	99 final	Combined
B01	$+0.32 \pm 0.20$	$+0.41 \pm 0.17$	$+0.28 \pm 0.14$	$+0.30 \pm 0.12$
B03	$+0.58 \pm 0.59$	-0.15 ± 0.63	-0.24 ± 0.60	$+0.12 \pm 0.42$

Table 3.1: Correction to $Re(\epsilon'/\epsilon)$ due to L3 loss as determined based on B01 and B03 reference triggers. Column "99 final" refers to the final 99 sample were the five L3 inefficient runs mentioned in the text are excluded. Note that for B03 reference trigger, since this trigger does not contain L2 condition, the bias corresponds to combine bias of L2 and L3.

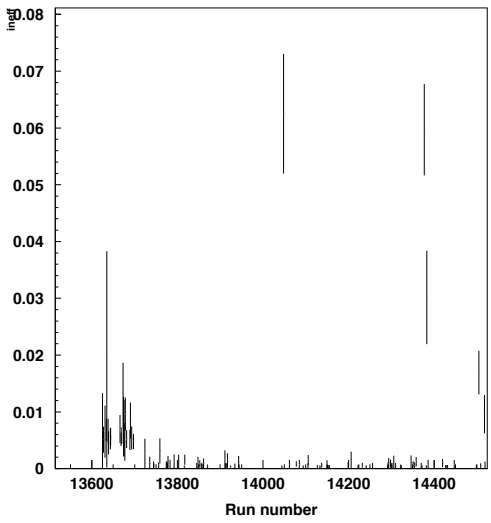

Figure 3.1: L3 efficiency, for Reg and Vac beam combined, as a function of run number as determined using B01 random accept events

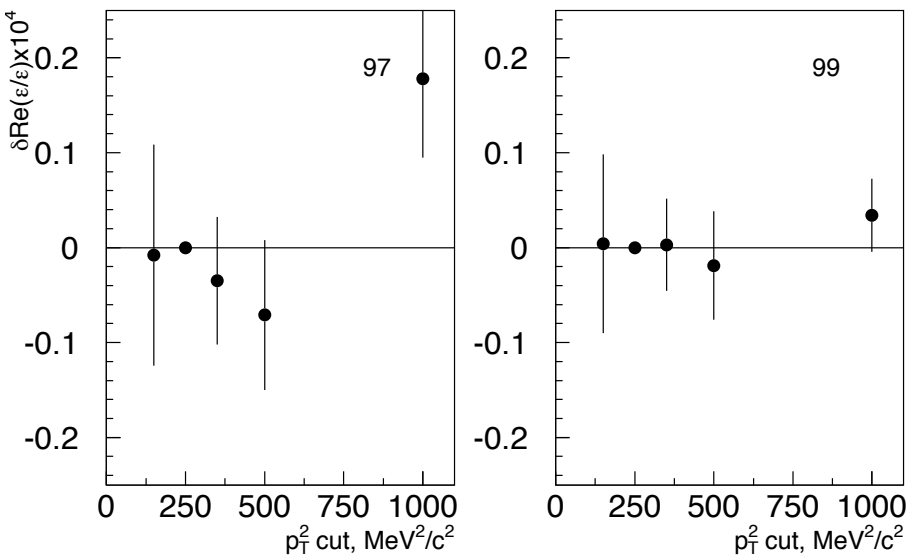

Figure 3.2: Variation of $Re(\epsilon'/\epsilon)$ for change in the $p_\perp^2$ cut.

Change of MC simulation	Bias in $Re(\epsilon'/\epsilon)$, $\times 10^4$	
No Scattering in Spectrometer	+0.19	-0.55
No DC maps	-0.87	-0.31
No Accidental Overlays	0.26	+0.03

Table 3.2: Variation of $Re(\epsilon'/\epsilon)$ for varios changes in MC simulation. For all test uncorrelated MC statistical uncertainty is 0.6×10^{-4}

3.1.2 Alignment and Calibration

$p_\perp$-kick, different alignment tests.

3.1.3 Selection Criteria

$p_\perp^2$, χ^2 and separation cuts. Other cuts.

3.1.4 DC efficiency and Resolution Modeling

3.1.5 Acceptance

Z overlay

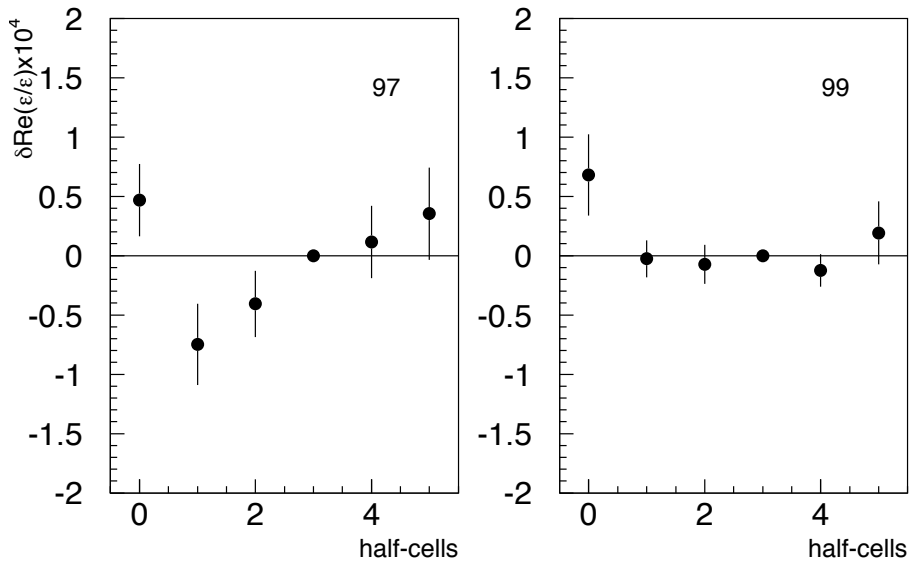

Figure 3.3: Variation of $Re(\epsilon'/\epsilon)$ for change in the cell separation cut.

3.1.6 Study of upstream $Z < Z_{MA}$ region

A special study has been performed for the upstream region of the Z vertex distibution, before the MA downstream edge. This region is prone to various systematic effects: pion scattering in MA, beam profile simulation, DC alignment and resolution. The studies are summarized in Table 3.3.

An overall check of the upstream region is performed by excluding $Z < Z_{MA}$ from the $Re(\epsilon'/\epsilon)$ fit (charged mode only). This cut changes and average Z vertex in Vac beam by +2.5 m. Therefore, for a Z slope a_Z a bias in $Re(\epsilon'/\epsilon)$ is expected to increase by $2.5/6a_Z$, if the slope by itself is not modified. The consitency of the restricted/whole Z range slopes is valid for all run periods. "Exepcted from Z_{av} change" change given in Table 3.3 is calculated assuming constant slope.

The change of $Re(\epsilon'/\epsilon)$ is statistically insignificant for 1997 data. For 1999 data, taking into account expected change in $Re(\epsilon'/\epsilon)$, there is 2.5σ additional bias in $Re(\epsilon'/\epsilon)$. For the combined data the bias has 1.9σ significance.

Another check consists of relaxing MA clearance cut. In this case the bias in $Re(\epsilon'/\epsilon)$ has an opposite sign for the two years, similarly to the change in Z vertex data to MC ratios, see Fig. 3.7. The change of the slope corresponds to -0.26 and $+0.67$ unit $Re(\epsilon'/\epsilon)$

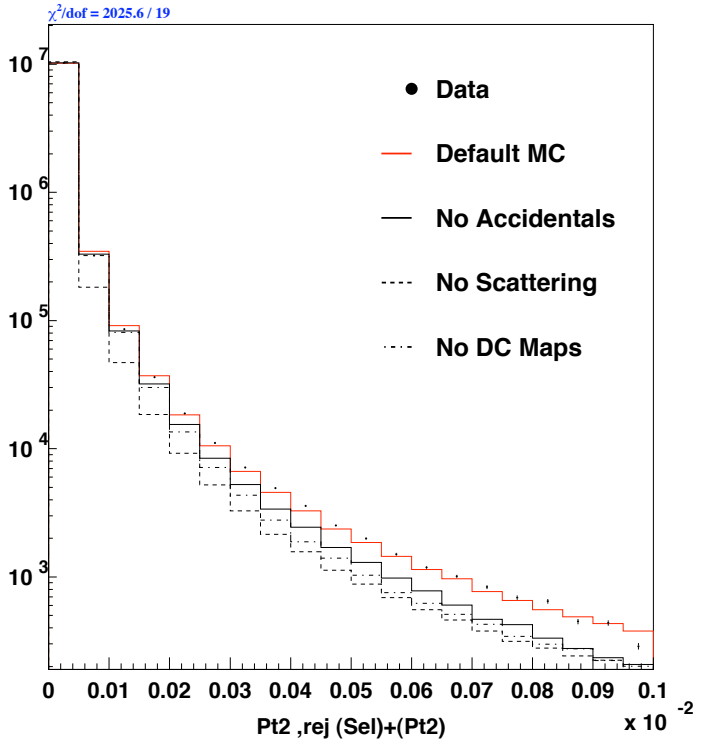

Figure 3.4: $p_\perp^2$ for Vac beam 1997 data compared to default MC simulation and MC with some of the smearing effects switched off.

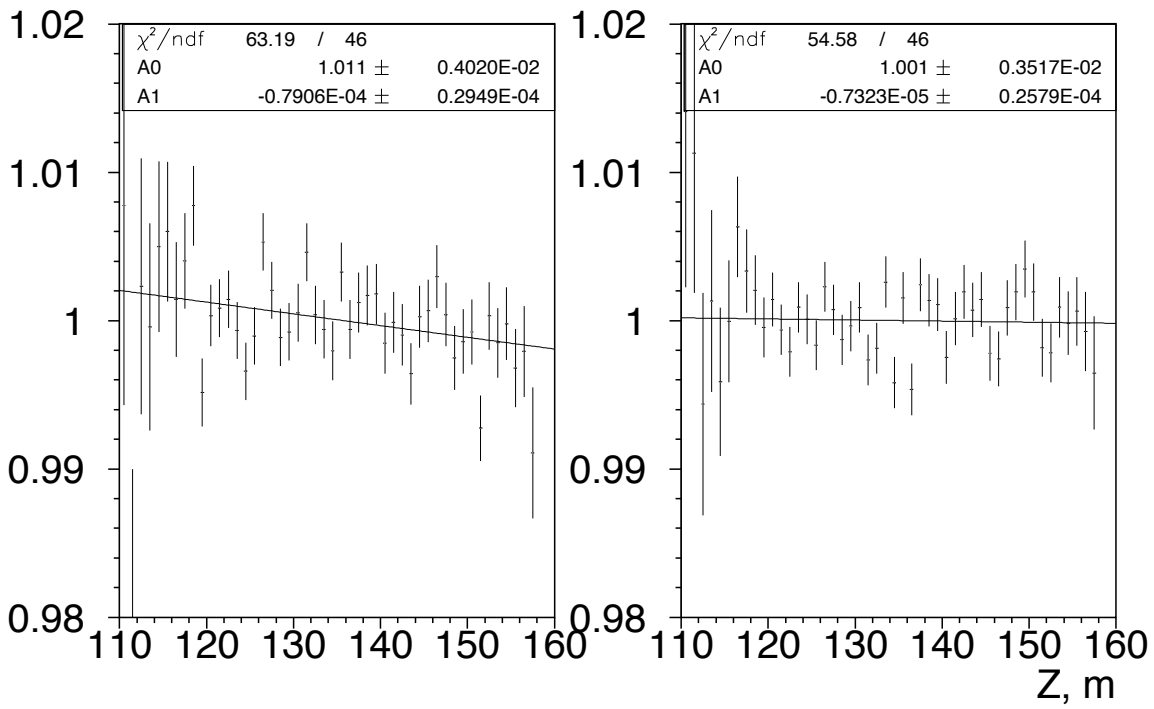

Figure 3.5: Ratio of Data to MC Z vertex distributions for events passing all cuts, 97 and 99 separatelly. If the fit region is restricted to $Z > 122.5$, the linear slope changes to $(-0.84 \pm 0.36) \times 10^{-4}$ for 97 data and $(+0.20 \pm 0.31) \times 10^{-4}$ for 99 data.

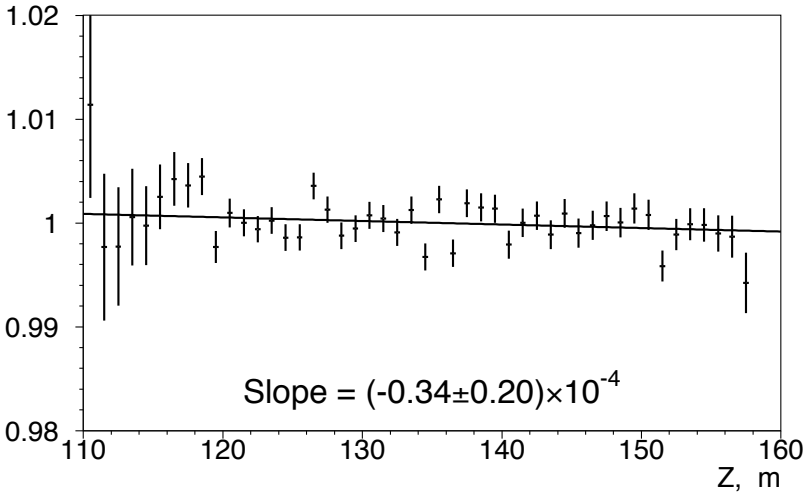

Figure 3.6: Ratio of Data to MC Z vertex distributions for events passing all cuts, 97 and 99 data combined. If the fit region is restricted to $Z > 122.5$, the linear slope changes to $(-0.24 \pm 0.24) \times 10^{-4}$.

Change in selection	Bias in $Re(\epsilon'/\epsilon)$, $\times 10^4$		
	97	99	Combined
$Z > 122.5$ m cut	-0.35 ± 0.33	-0.40 ± 0.24	-0.41 ± 0.18
expected from Z_{ave} change	-0.33	-0.03	-0.10
No MA clearance cut	$+0.24 \pm 0.12$	-0.84 ± 0.10	-0.38 ± 0.07
expected from Z slope change	-0.05	$+0.27$	$+0.10$

Table 3.3: Variation of $Re(\epsilon'/\epsilon)$ for different cuts for the upstream Z region

change, which is similar in size to the observed variation but has opposite sign. The wrong sign is expected: for example, loss of events localized to upstream of MA affects Vac beam only (decrease of $Re(\epsilon'/\epsilon)$) but the Z slopes becomes more postive which suggests larger losses for upstream Z in general and thus larger loss in Reg beam (increase of $Re(\epsilon'/\epsilon)$) since Reg beam has on average smaller Z.

3.1.7 Background Subtraction

3.1.8 Cross checks

Run dependence, in/out-bends, perfect/problematic tracking.

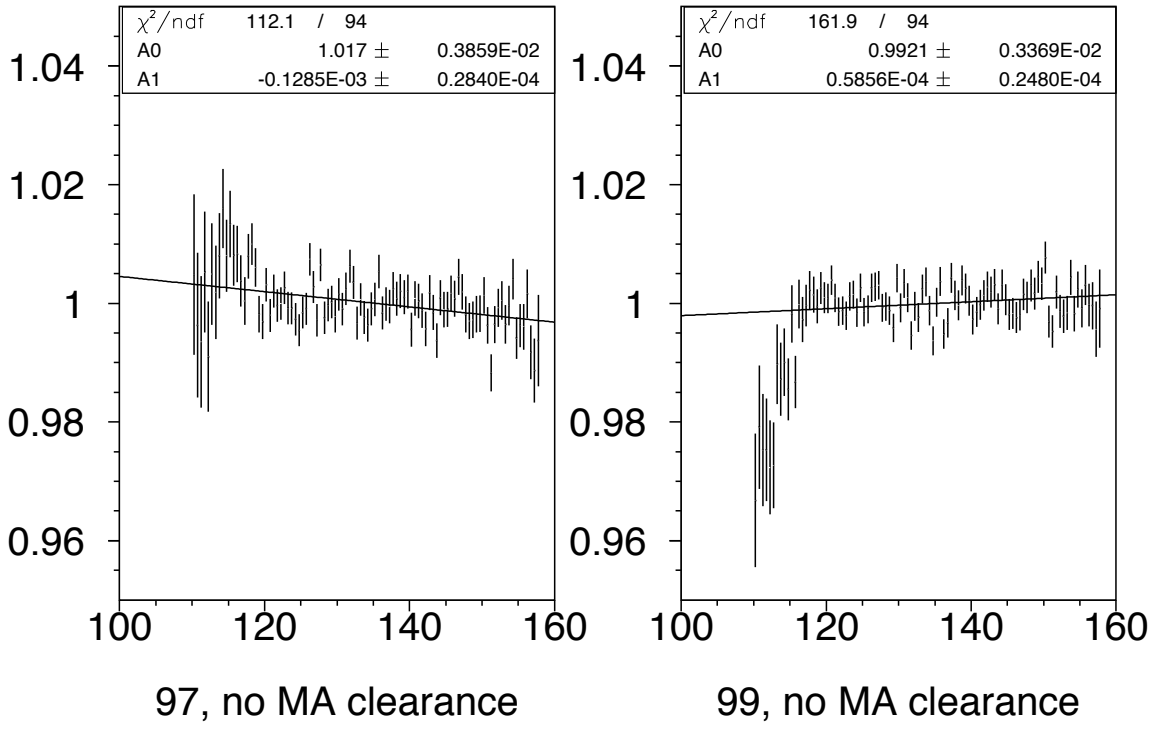

Figure 3.7: Ratio of Data to MC Z vertex distributions for events passing all cuts excluding cut on MA clearance

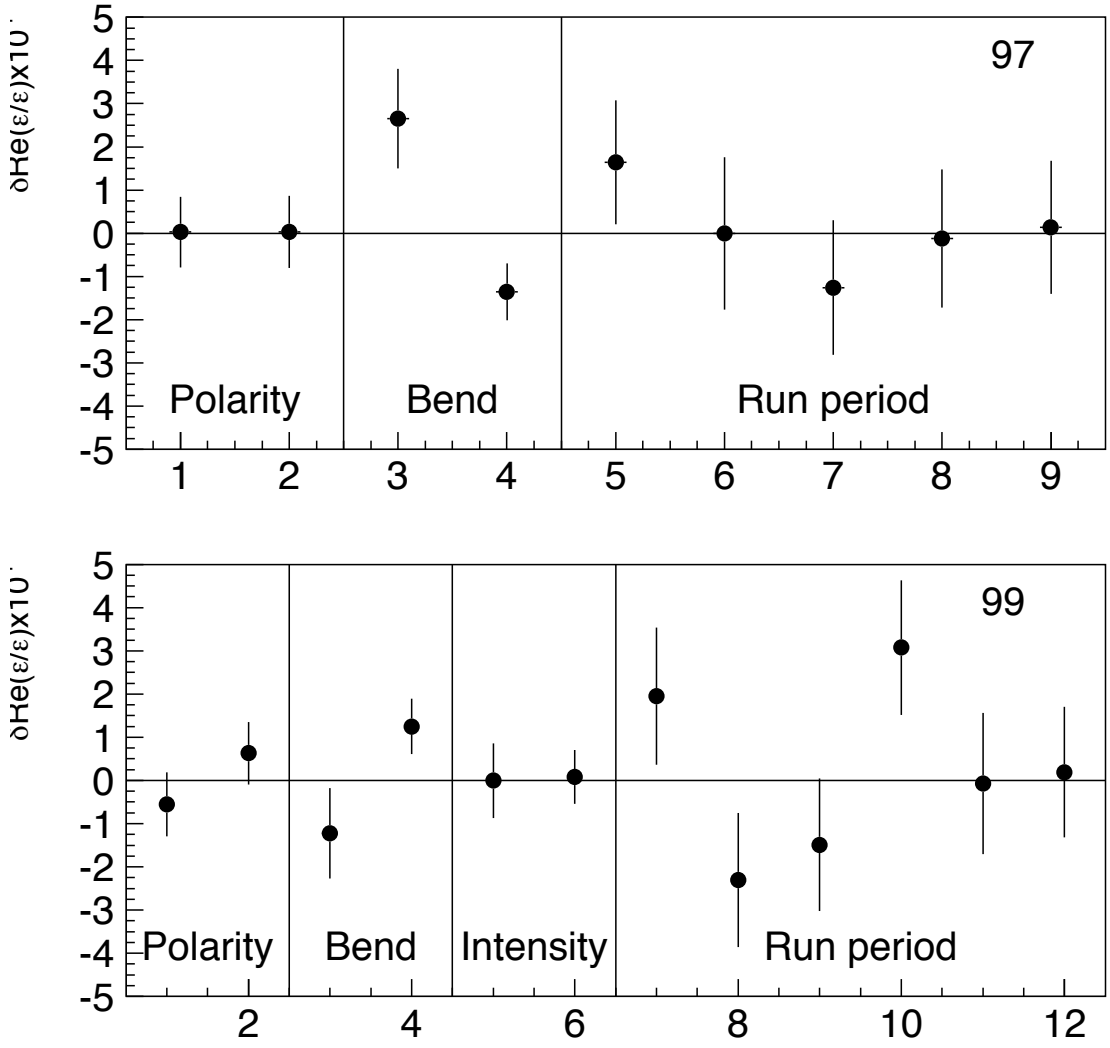

Figure 3.8: Cross checks of $Re(\epsilon'/\epsilon)$ measurement. Points labeled "Polarity", "Bend", "Intensity" correspond to the data sets split into halfs based on (from left to right) positive/negative magnet polarity, in/out bending topology, low, $< 5 \times 10^{12}$/high, $> 5 \times 10^{12}$ intensity. Points labeled "run period" corresponds to data split into 5 (for 1997) or 6 (for 1999) sub-periods. The same fixed neutral mode data is used for all tests. The errors are estimated by difference vs nominal sample in quadrature.

Source	Uncertainty $\times 10^{-4}$			
	97 PRD	97	99	Combined
Online selection				
L1 and L2	0.20			??
L3	0.54	0.17 (0.42)	0.14 (0.35)	0.12(0.36)
Track reconstruction				
Alignment and Calibration	0.28	0.20	0.20	0.20
Momentum scale	0.16	0.10	0.10	0.10
Selection efficiency				
$p_\perp^2$ cut	0.25	0.10	0.10	0.10
DC efficiency modeling	0.37	0.15	0.15	0.15
DC resolution modeling	0.15	0.15	0.15	0.15
Apertures				
Wire spacing	0.22	0.22	0.22	0.22
Effective regenerator edge	0.20	0.20	0.20	0.20
Z-slope	0.79	0.87	0.25	0.41
Z-upstream	—	0.33	0.48	0.40
Background subtraction	0.20	0.20	0.20	0.20
Monte Carlo statistics	0.41	0.26	0.25	0.20
Total Systematics	1.26	1.11 (1.18)	0.81 (0.87)	0.81 (0.88)
Stat. Charged	0.65	0.68	0.58	0.45
Total Charged	1.41	1.30 (1.18)	0.99 (1.04)	0.93 (0.99)

Table 3.4: Summary of the systematic uncertainties. L3 bias is applied as correction, see Table 3.1. Number in parenthesis corresponds to the error if L3 bias is not corrected but attributed to the uncertainty.

Chapter 4

CPT Tests

4.1 Systematic Uncertainties

Table 4.1: Results of the Z binned fits . The errors correspond to stat. errors only.

	PRD	97	99	Combined
		SW phase fit		
$\Delta M \times 10^6 \hbar s^{-1}$	5266.7 ± 5.9	5267.3 ± 6.3	5270.2 ± 5.5	5269.0 ± 3.9
$\tau_S \times 10^{-12} s$	89.650 ± 0.028	89.637 ± 0.029	89.609 ± 0.026	8962.0 ± 0.018
		CPT fit		
$\Delta M \times 10^6 \hbar s^{-1}$	5288 ± 23	5293 ± 22	5288 ± 19	5290 ± 14
$\tau_S \times 10^{-12} s$	89.58 ± 0.08	89.56 ± 0.07	89.55 ± 0.06	89.55 ± 0.05
ϕ_{+-}	$[44.12 \pm 0.72]^o$	$[44.22 \pm 0.67]^o$	$[44.00 \pm 0.6227]^o$	$[44.09 \pm 0.43]^o$
		$\phi_{+-} - \phi_{SW}$ fit		
$\delta\phi$	$[+0.61 \pm 0.62]^o$	$[+0.70 \pm 0.58]^o$	$[+0.51 \pm 0.50]^o$	$[+0.58 \pm 0.38]^o$

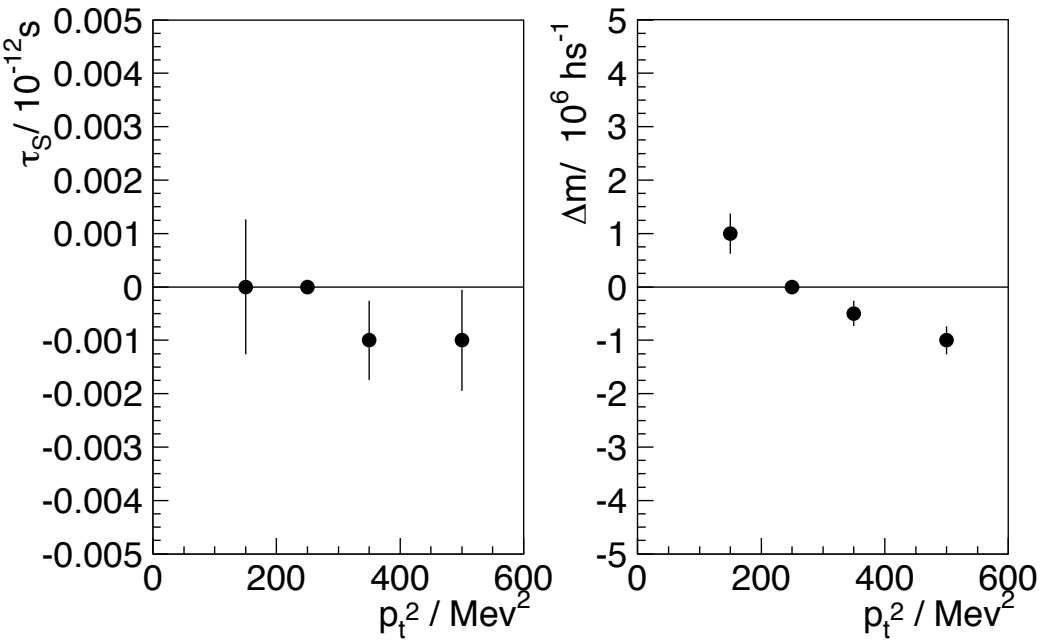

Figure 4.1: Variation of ΔM (right) and τ_S (left) for different p_t^2 cuts

Table 4.2: Systematic uncertainties in ΔM, τ_S in PRD and in the combinded 97-99 analysis.

	PRD		Combined 97 and 99	
Source	ΔM	τ_S	ΔM	τ_S
Trigger ??	0.2	0.004	0.2	0.004
Track reconstruction	0.6	0.032 (0.008?)		
maps			-0.4	+0.002
resolution			-0.5	+0.007
p_t kick			-0.6	+0.008
Z DC			-0.1	+0.001
Selection efficiency	3.2	0.011		
pt cut			-1.0	-0.001
accidental			+0.2	-0.001
scattering			-0.5	+0.001
Apertures (Track separ)	2.8	0.038	-2.0	+0.011
Background	0.8	0.002	2.0	0.002
Acceptance	1.2	0.026		
Z slope			0.2	-0.014
MC statistics	2.6	0.012	1.5	0.007
Fitting	13.3	0.045		
Attenuation	10.0	0.020		
Attenuation Norm			+0.7	-0.004
Attenuation Slope			-4.5	+0.011
Target K_S	1.4	0.017	1.4	-0.017
Screening	3.0	0.020	3.0	0.020
Analytisity	8.1	0.030	8.1	-0.030
τ_L	0.0	0.001	0.0	0.000
Total Syst	14.3	0.074 (0.066?)	10.5	0.047
Stat Error	5.9	0.028	3.9	0.018
Total Error	15.4	(0.072?)	11.2	0.051

Table 4.3: Systematic uncertainties in ΔM, τ_S, ϕ_{+-} in PRD and in the combinded 97-99 analysis.

	PRD			Combined 97 and 99	
Source	ΔM	τ_S	ϕ_{+-}	ΔM	τ_S	ϕ_{+-}
Trigger ??	-3.0	0.006	-0.10			
Track reconstruction	-1.0	0.008	-0.02			
maps				0.0	0.000	0.00
resolution				-2.6	0.001	-0.08
p_t kick				-0.7	+0.009	0.00
Z DC				-0.1	+0.002	0.00
Selection efficiency	+8.8	-0.029	+0.35			
pt cut				-3.2	+0.006	-0.08
accidental				0.1	0.000	0.02
scattering				-0.3	0.001	-0.10
Apertures	-24.	0.054	-0.76			
track separation				-10.6	+0.039	-0.33
Background	0.0	0.001	0.01	0.0	0.001	0.01
Acceptance	-5.9	-0.020	-0.14			
Z slope				-1.6	-0.007	-0.06
MC statistics	9.2	0.030	0.28	5.1	0.016	0.16
Fitting						
Attenuation						
Attenuation Norm	+1.1	-0.014	-0.06	+0.3	-0.003	-0.01
Attenuation Slope	-7.0	-0.012	+0.006	-2.4	+0.004	+0.05
Target K_S	+4.7	-0.026	0.11	+4.7	-0.026	0.11
Screening	-20.7	+0.056	-0.75	-20.7	+0.056	-0.75
Analytisity	0.0	0.00	0.25	0.0	0.00	0.25
τ_L	0.0	0.00	0.00	0.0	0.00	0.00
Total Syst			1.20	24.97	0.076	0.90
Stat Error	23	0.080	0.72	14.13	0.046	0.43
Total Err	42	0.130	1.40	28.63	0.089	1.00

Table 4.4: Systematic uncertainties in $\Im(\epsilon'/\epsilon)$, $\Re(\epsilon'/\epsilon)$ in PRD and in the combinded 97-99 analysis.

	PRD		Combined 97 and 99	
Source	$\Re(\epsilon'/\epsilon)$	$\Im(\epsilon'/\epsilon)$	$\Re(\epsilon'/\epsilon)$	$\Im(\epsilon'/\epsilon)$
Trigger ??	-0.14	-1.16		
Track reconstruction	-0.14	+1.70		
maps			0.04	0.48
resolution			0.10	-1.20
p_t kick			-0.14	1.75
Z DC			-0.28	0.39
Selection efficiency	-0.42	-3.3		
pt cut			-0.17	+1.11
accidental			+0.05	-0.73
scattering			-0.15	+0.17
Apertures (Track separ)				
Cell separation	-0.31	-3.32	-0.47	+2.76
Calo separation	-0.41	+3.69	-0.33	+3.65
Background	0.1	0.6	0.1	0.6
Acceptance	-0.36	-3.49		
Z slope			-0.11	+3.04
MC statistics	0.37	2.60	0.24	1.57
Fitting	0.05	+0.28		
Attenuation				
Attenuation Norm			0.00	0.02
Attenuation Slope			0.03	0.14
Target K_S				
Screening	-0.01	-1.44	-0.01	-1.44
Analytisity				
τ_L				
Total Syst			0.77	6.57
Stat Error			0.54	3.53
Total Error			0.94	7.46

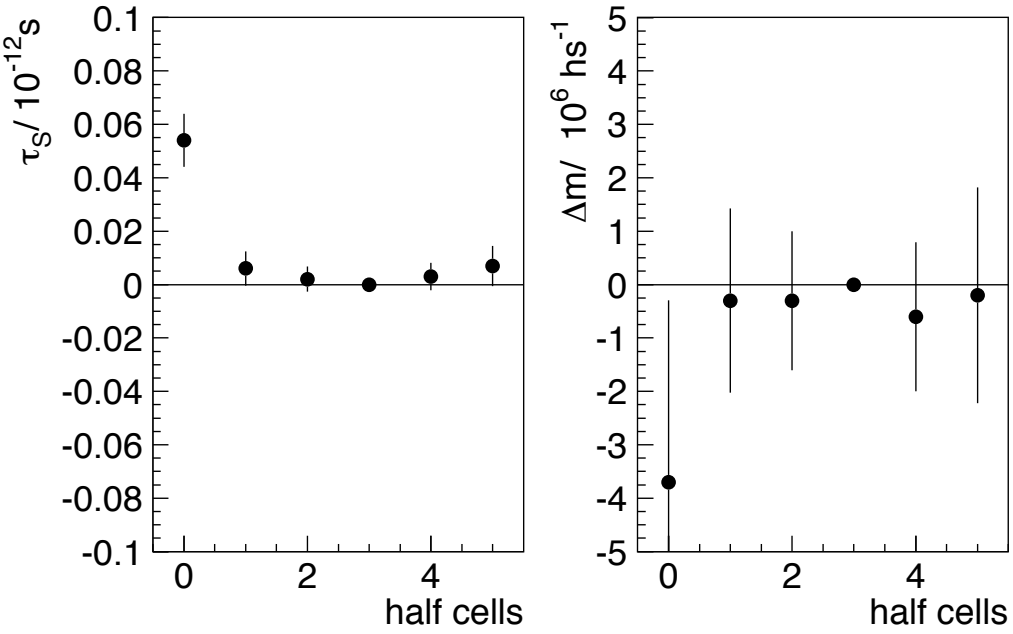

Figure 4.2: Variation of ΔM (right) and τ_S (left) as a function of cell separation cut

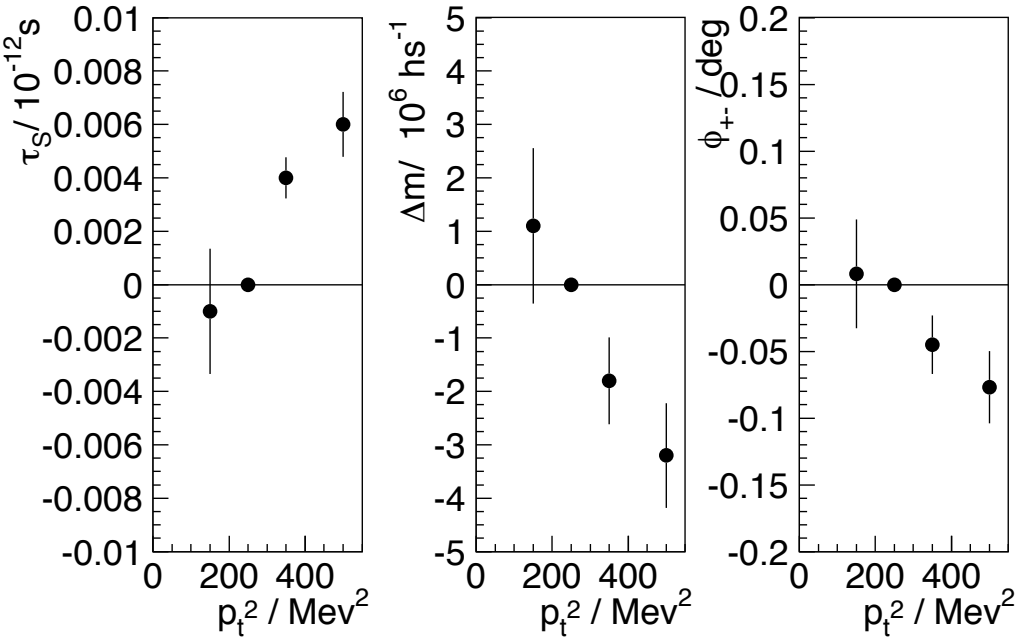

Figure 4.3: Variation of τ_S, ΔM, ϕ_{+-} for different p_t^2 cuts

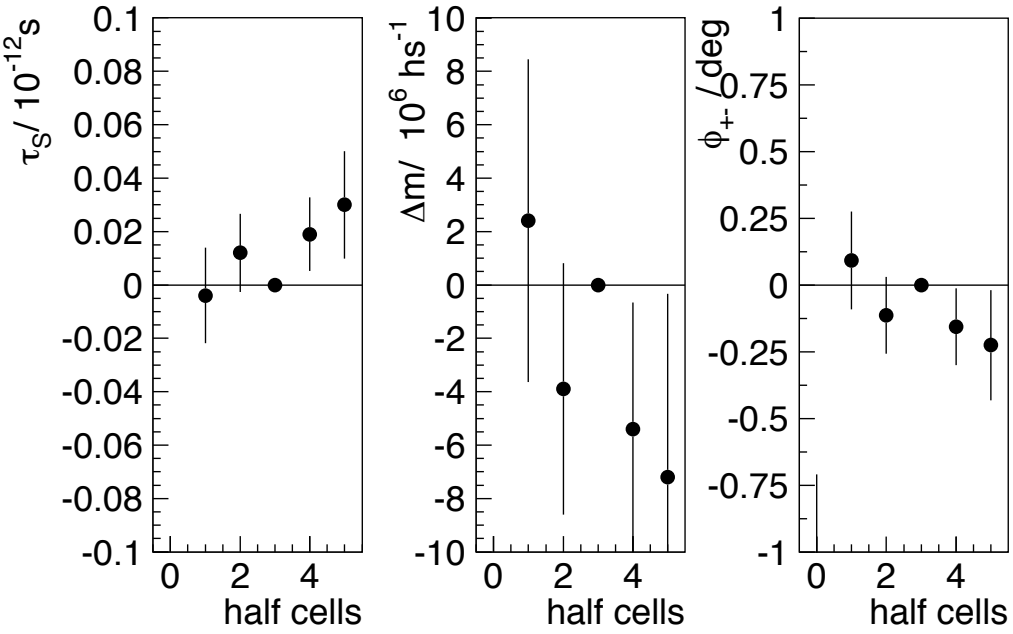

Figure 4.4: Variation of τ_S, ΔM, ϕ_{+-} as a function of cell separation cut

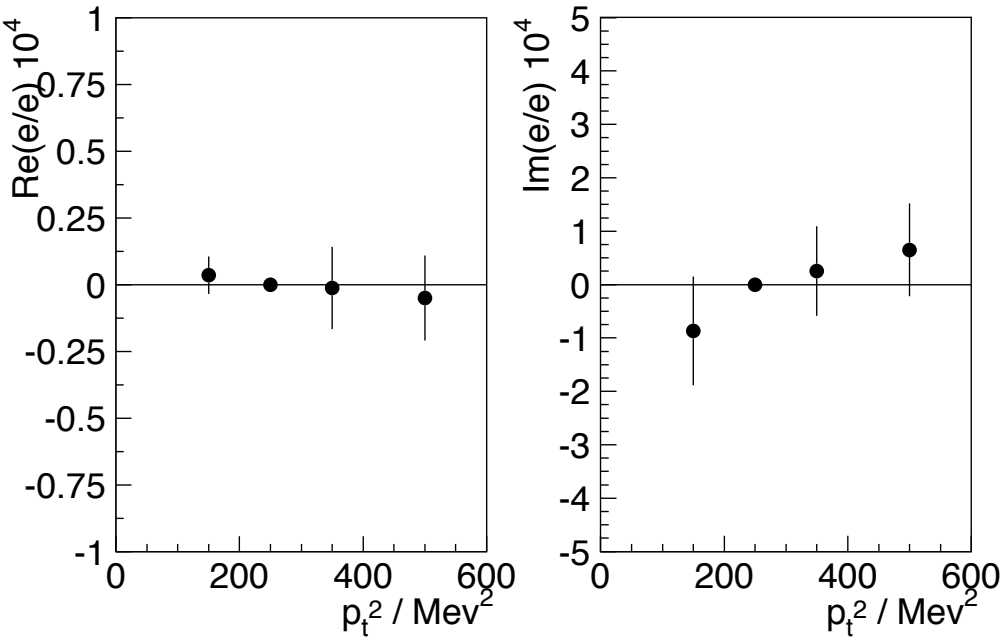

Figure 4.5: Variation of $Re(\epsilon'/\epsilon)$ (left) and $Im(\epsilon'/\epsilon)$ (right) for different p_t^2 cuts

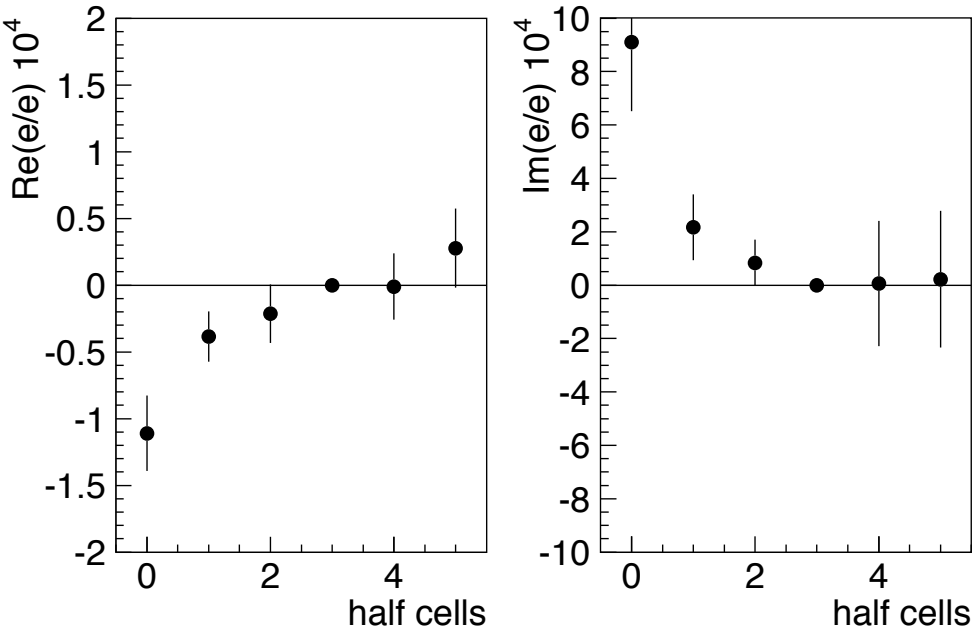

Figure 4.6: Variation of $Re(\epsilon'/\epsilon)$ (left) and $Im(\epsilon'/\epsilon)$ (right) as a function of cell separation cut

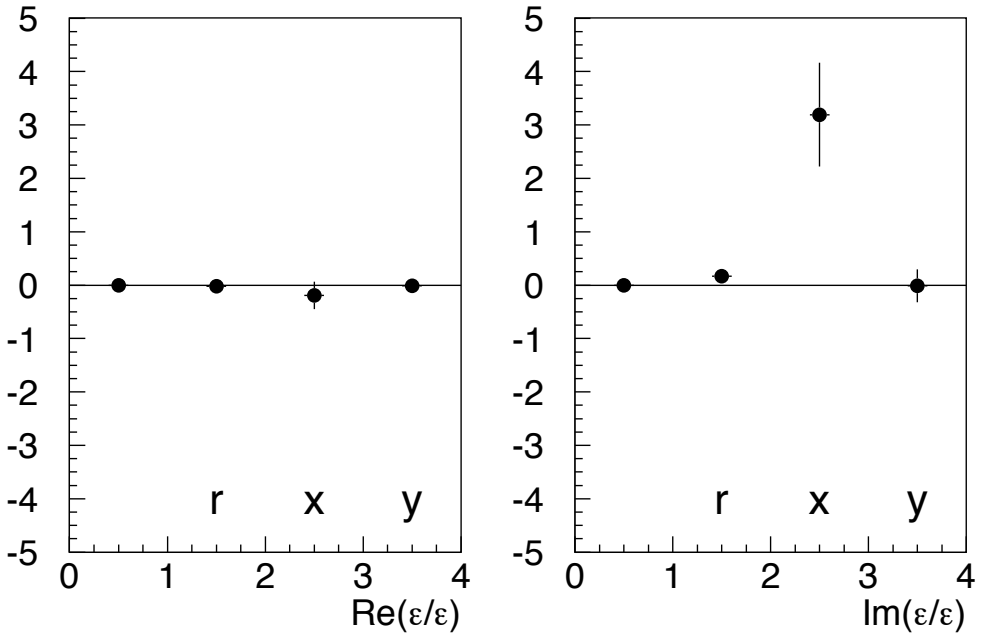

Figure 4.7: Variation of $Re(\epsilon'/\epsilon)$ (left) and $Im(\epsilon'/\epsilon)$ (right) if the calorimeter track separation cuts are relaxed.

Appendix A

Selection Cuts

Appendix B

Background Subtraction Control Plots

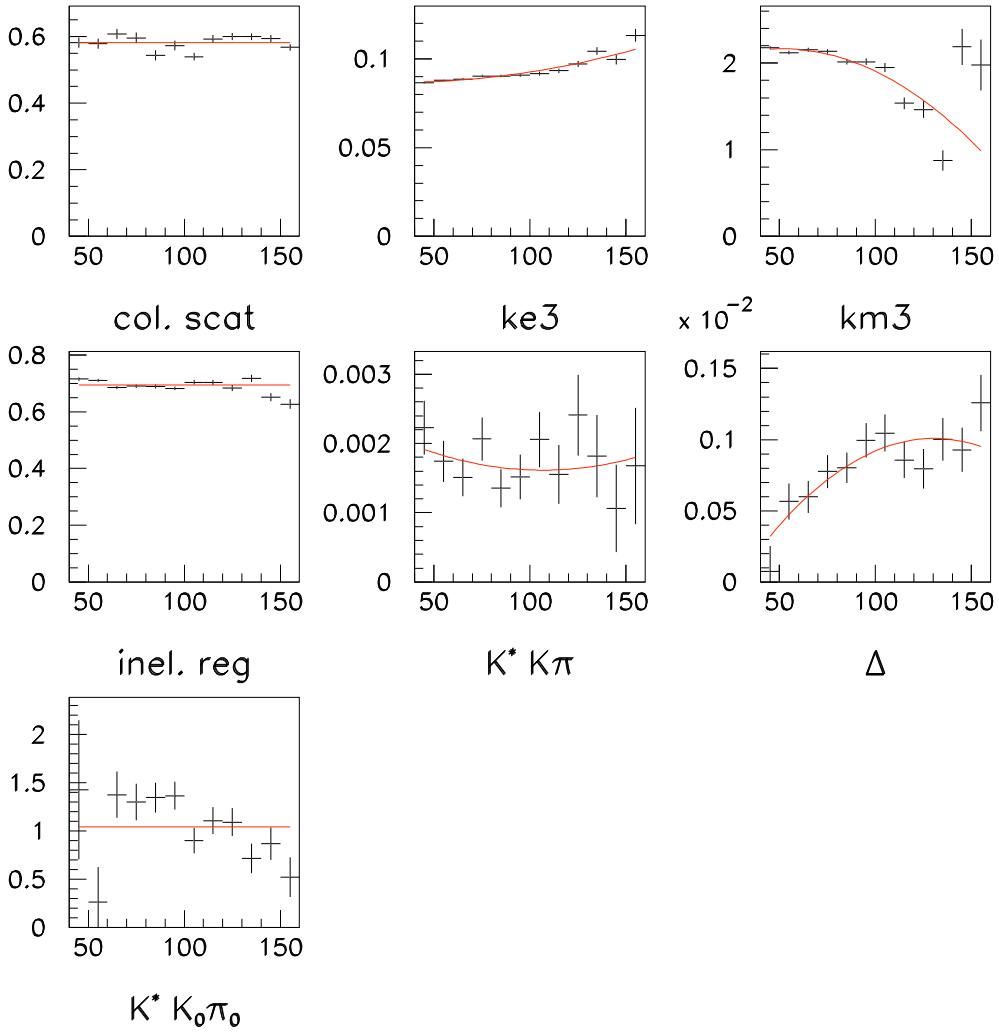

Figure B.1: Momentum dependent normalization of the different background components (from left to right: collimator scattering, K_{e3}, $K_{\mu 3}$, inelastic regenerator scattering, $K^* \to K^{\pm}\pi^{\mp}$, $\Delta \to p^{\pm}\pi^m p$, $K^* \to K_S\pi^0, K_S \to \pi^+\pi^-$). Dots are based on fits to 1999 data. Line indicate second order polynomial fit used for background normalization.

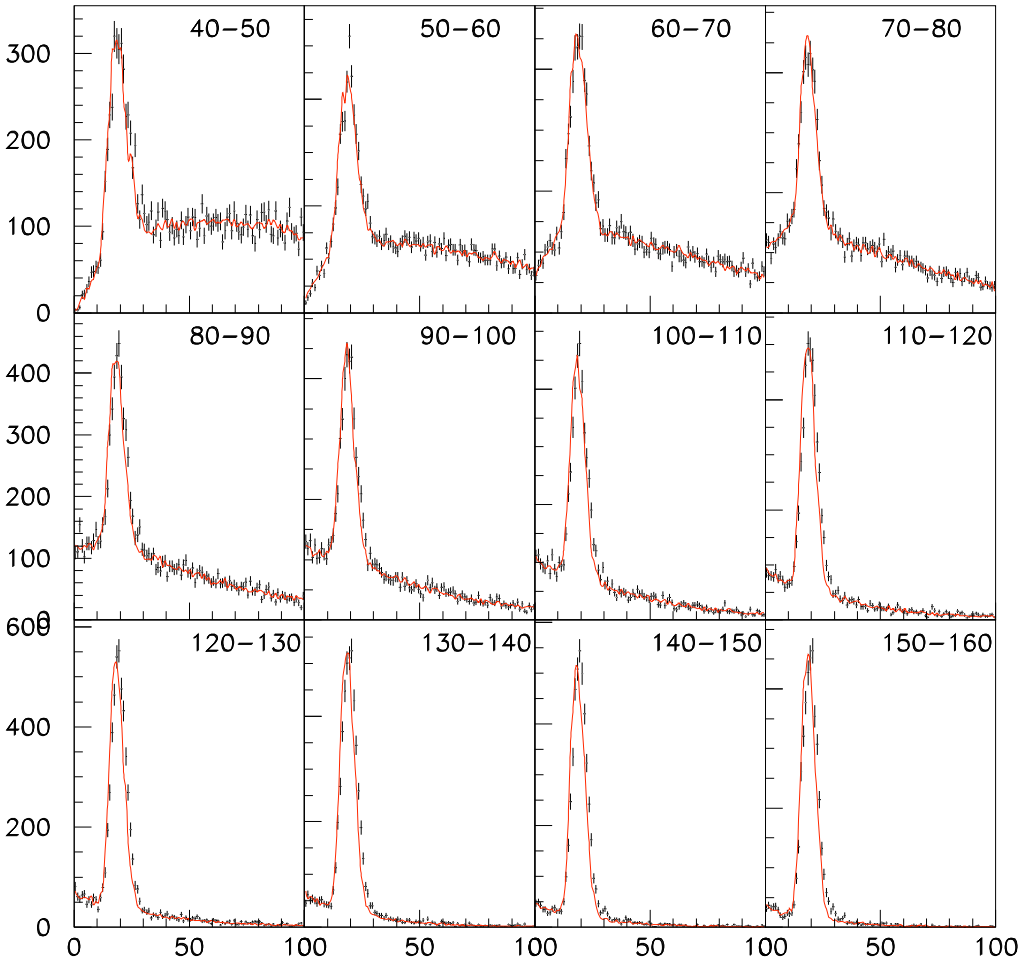

Figure B.2: E_K dependent normalization of collimator scattering background. Plots show collimator ring distribution for high $p_\perp$ events in Vacuum beam. The peak corresponds to collimator scattering background, the sidebands are from K_{e3}, $K_{\mu 3}$ and resolution tails

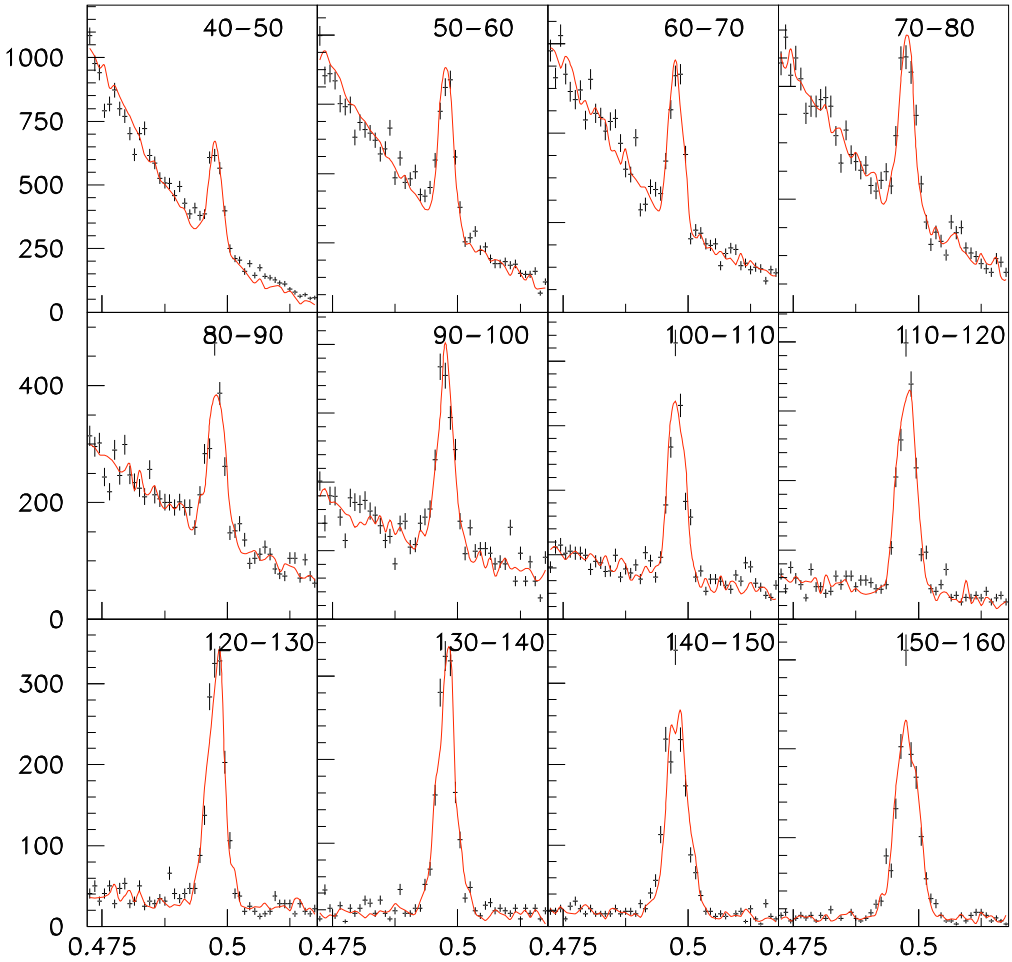

Figure B.3: E_K dependent normalization of K_{e3} background. The plot is based on "double Shower selection", 1999 data. The peak around the nominal K^0 mass corresponds to collimator scattering background. K_{e3} normalization is determined from the mass sidebands

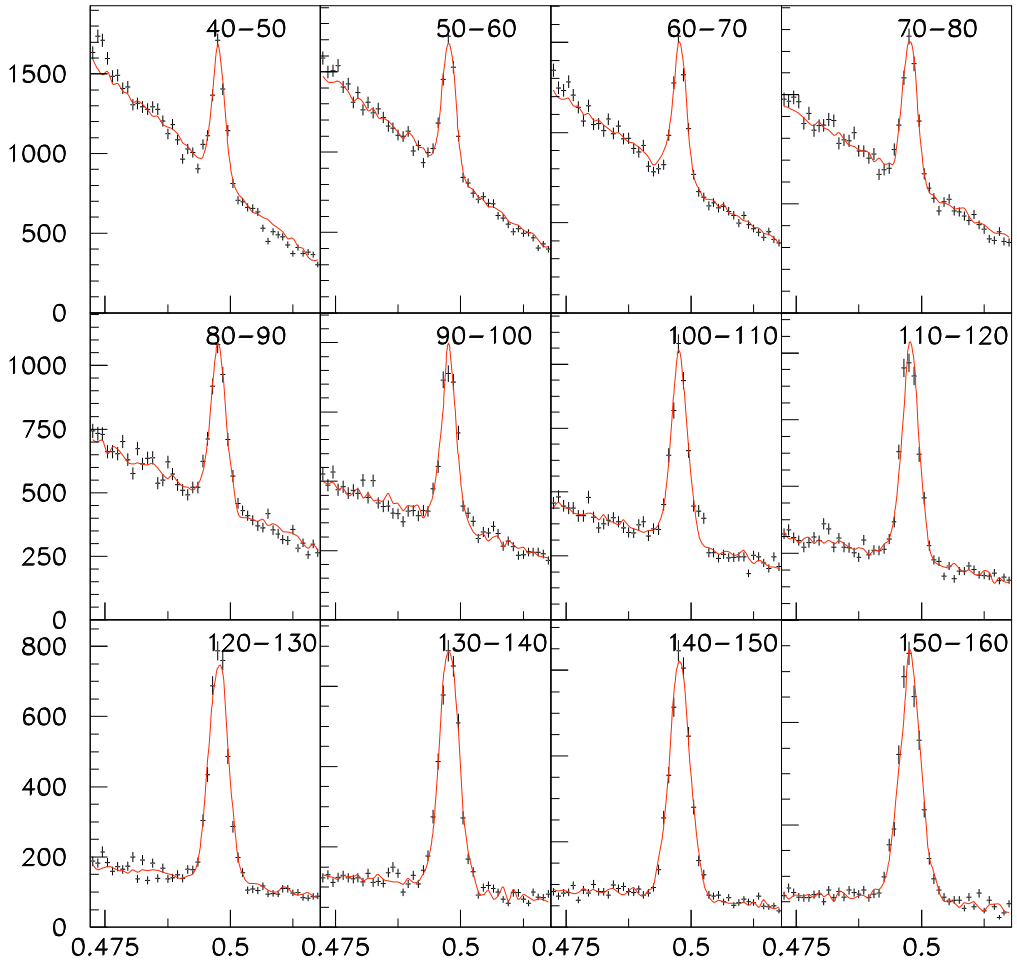

Figure B.4: E_K dependent normalization of $K_{\mu 3}$ background. The plot is based on "double MIP selection", 1999 data. The peak around the nominal K^0 mass corresponds to collimator scattering background. $K_{\mu 3}$ normalization is determined from the mass sidebands

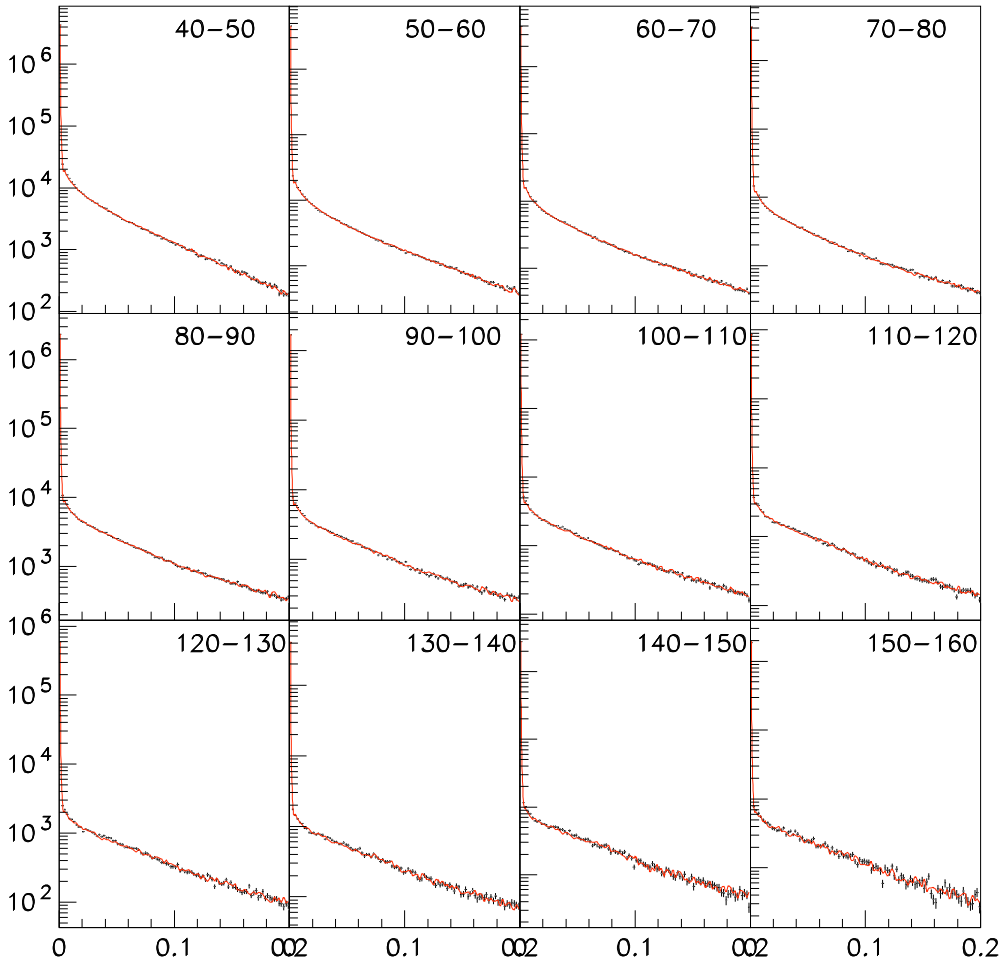

Figure B.5: Normalization of $K^* \rightarrow K_S\pi^0, K_S \rightarrow \pi^+\pi^-$ and inelastic reg. scattering background. The plots show $p_\perp$ distribution in E_K bins for Regenerator beam.

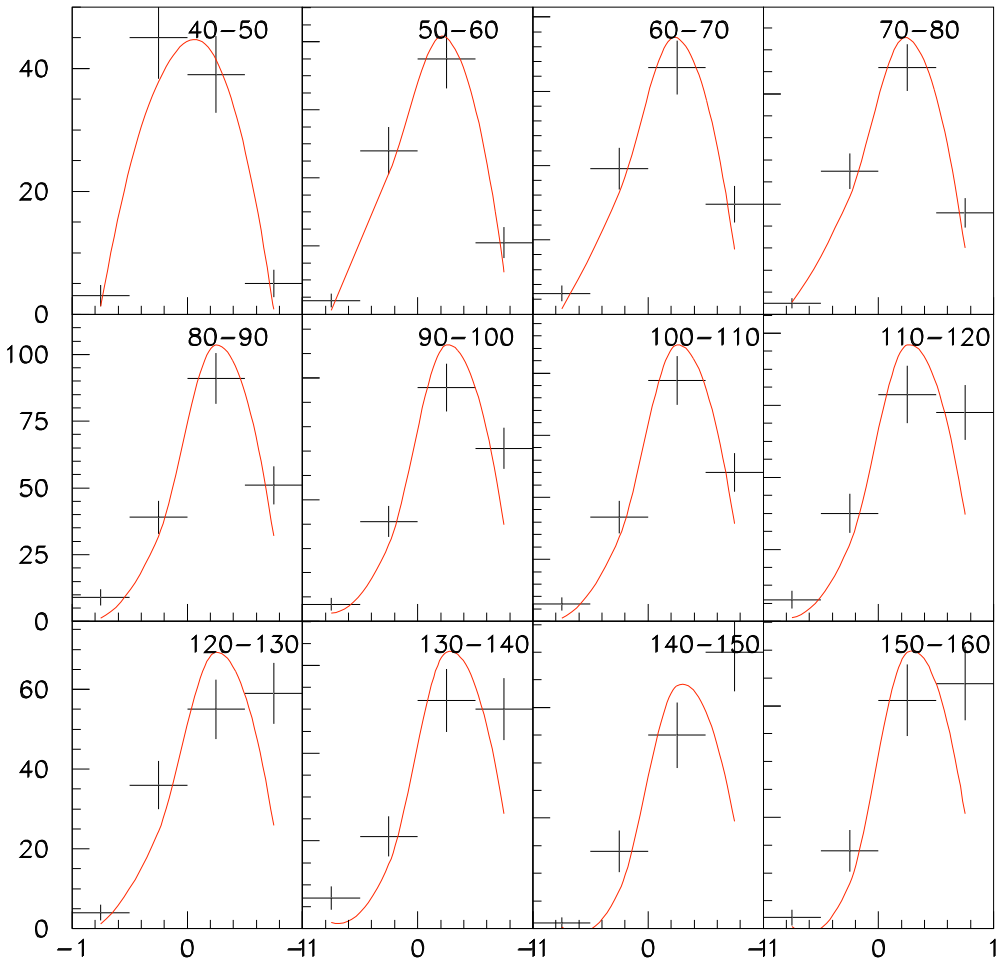

Figure B.6: Normalization of K^* and Δ background. The plots show momentum asymmetry distribution for Regenerator beam near the Regenerator edge, mass sidebands. Larger asymmetry for high momentum bins correspond to larger contribution of Δ resonance.